

# Dielectric and Mechanical Properties of PDMS–La<sub>2</sub>Ba<sub>2</sub>XZn<sub>2</sub>Ti<sub>3</sub>O<sub>14</sub> (X = Mg/Ca/Sr) Nanocomposites

Suryakanta Nayak,<sup>\*∇</sup> Banalata Sahoo,<sup>∇</sup> Tapan Kumar Rout, and Amar Nath Bhagat



Cite This: *ACS Omega* 2023, 8, 37090–37097



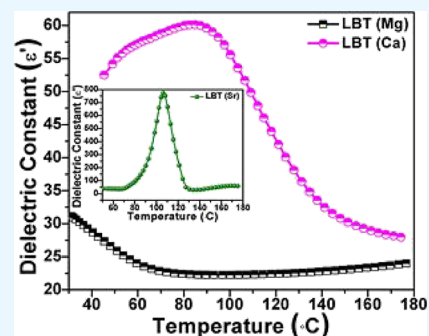
Read Online

ACCESS |

Metrics & More

Article Recommendations

**ABSTRACT:** Flexible polydimethylsiloxane–La<sub>2</sub>Ba<sub>2</sub>XZn<sub>2</sub>Ti<sub>3</sub>O<sub>14</sub> (X = Mg/Ca/Sr) [PDMS–LBT] nanocomposites with high permittivity (dielectric constant,  $k$ ) are prepared through a room-temperature mixing process. The LBT nanoparticles used in this study are prepared through a high-temperature solid-state reaction. It is observed that LBT (X = Mg/Ca) nanoparticles are spherical in nature, with particle size  $\sim 20$  nm, as observed from the HRTEM images, whereas LBT (X = Sr) nanoparticles are cubical in nature with particle size  $\geq 100$  nm. These LBT (X = Mg/Ca/Sr) nanoparticles are crystalline in nature, as apparent from the XRD analysis and SAED patterns. The permittivity of LBT nanoparticles is higher when “Ca” is present in place of “X”. These three oxides show a temperature-dependent dielectric behavior, where LBT nanoparticles with “Sr” show a sharp change in permittivity at a temperature of  $\sim 105$  °C. These kinds of oxide materials, especially LBT (X = Sr) nanoparticles/oxides, can be used in dielectric/resistive switching devices. The effect of LBT nanoparticle concentration on the dielectric and mechanical properties of PDMS–LBT nanocomposites is widely studied and found that there is a significant increase in dielectric constant with an increase in the concentration of LBT nanoparticles. There is a decrease in the volume resistivity with the increase in the LBT nanoparticle concentration. All the PDMS–LBT nanocomposites have low dielectric loss ( $\epsilon''$ ) compared to the dielectric constant value. It is found that both permittivity ( $\epsilon'$ ) and AC conductivity ( $\sigma_{ac}$ ) of PDMS–LBT composites are increased with the temperature at a frequency of 1 Hz. The % elongation at break (% EB) and tensile strength (TS) decrease with the LBT nanoparticle concentration in the matrix PDMS, which is due to the non-reinforcing behavior of LBT nanoparticles. The distribution and dispersion of LBT nanoparticles in the matrix PDMS are observed through HRTEM and AFM/SPM.



## 1. INTRODUCTION

Polymer composites (particle-reinforced polymer) have shown great interest because the addition of filler particles to a matrix polymer can enhance the electrical, thermal, mechanical, barrier, and other various properties.<sup>1–34567</sup> These composites may contain oxide/inorganic particles, nanofibers, nanoclays, carbon powder/fillers, carbon nanotubes, or graphene dispersed in appropriate matrix polymers.<sup>1,3,8–10111213141516</sup> Polymer composites have different applications in the field of electronic materials such as photovoltaic devices, capacitors, actuators, electromagnetic interference (EMI) shielding, static charge dissipation, angular acceleration accelerometers, acoustic emission sensors, electronic packaging materials, and integrated decoupling capacitors.<sup>1,3,8,13,17–19</sup> There are many processing advantages of these polymer composite materials, which include mechanical flexibility and can be molded into various complex shapes/geometries. Therefore, polymers/polymer composite materials can be used in compact electronics.<sup>17,20</sup>

In the past decades, polymer–ceramic composites/nanocomposites have been of great interest to researchers for their novel applications. There are various ceramic oxides/particles which have been used by different research groups in making

polymer composites for various applications.<sup>21–23242526</sup> However, there is an increase in demand for electroceramic oxide fillers in making polymer composites due to their various electrical properties.<sup>27–29303132</sup> Technically, these special classes of ceramic oxides have been explored for their ferroelectric, piezoelectric, and dielectric responses and have been used in nonvolatile memories [dynamic random access memories (DRAMs)], high-capacity dielectric devices, and materials for energy storage and conversion.<sup>33–35</sup> The incorporation of these electroceramic fillers in the matrix polymer has become a common practice to improve the electrical, mechanical, and other properties. These polymer–ceramic composites/nanocomposites can be effectively used as flexible electronic and electrical materials.<sup>36</sup>

Received: June 26, 2023

Accepted: August 2, 2023

Published: September 25, 2023



There is no literature based on PDMS nanocomposites using LBT ( $X = \text{Ca}, \text{Mg}, \text{and Sr}$ ) as electroceramic fillers. There are only two reports based on  $\text{Ln}_2\text{Ba}_2\text{CaZn}_2\text{Ti}_3\text{O}_{14}$  ( $\text{Ln} = \text{La}$  and  $\text{Pr}$ ) and  $\text{Nd}_2\text{Ba}_2\text{CaZn}_2\text{Ti}_3\text{O}_{14.4}$  ceramic oxides.<sup>37,38</sup> In the present study, we have prepared similar oxides by varying the reactant at the position of “Ca” and “Ln/Nd” by “Mg/Ca/Sr” and “La”, respectively. We have prepared LBT ( $X = \text{Mg}, \text{Ca}, \text{or Sr}$ ) electroceramic oxides (nanoparticles) using three different reactants such as  $\text{CaCO}_3$ ,  $\text{MgO}$ , and  $\text{SrCl}_2 \cdot 6\text{H}_2\text{O}$  along with  $\text{La}_2\text{O}_3$ ,  $\text{BaCO}_3$ ,  $\text{ZnO}$ , and  $\text{TiO}_2$ . The present paper describes the preparation of LBT ( $X = \text{Mg/Ca/Sr}$ ) nanoparticles through a high-temperature solid-state reaction using stoichiometric amounts of  $\text{La}_2\text{O}_3$ ,  $\text{BaCO}_3$ ,  $\text{CaCO}_3$ ,  $\text{MgO}$ ,  $\text{SrCl}_2 \cdot 6\text{H}_2\text{O}$ ,  $\text{ZnO}$ , and  $\text{TiO}_2$ . The shapes of different LBT ( $X = \text{Mg/Ca/Sr}$ ) nanoparticles are studied by HRTEM. Both room-temperature and temperature-dependent dielectric properties are discussed in detail. The crystal structures of these nanoparticles are determined through X-ray diffraction analysis. This paper also describes the preparation of nanocomposites using polydimethylsiloxane (PDMS) elastomer as the base matrix and the prepared LBT ( $X = \text{Mg/Ca/Sr}$ ) particles as fillers. The mechanical and dielectric properties of these nanocomposites are studied as a function of filler concentration and frequency. The temperature-dependent dielectric properties are studied at a frequency of 1 Hz. The distribution and dispersion of LBT ( $X = \text{Mg/Ca/Sr}$ ) nanoparticles in the PDMS matrix are studied by atomic force microscopy (AFM)/scanning probe microscopy (SPM) and HRTEM.

## 2. EXPERIMENTAL SECTION

**2.1. Materials.** The base matrix [polydimethylsiloxane (PDMS) elastomer] used in the present study was procured from D J Silicone. The density and shore-A hardness of the PDMS elastomer were  $1.12 \text{ g/cm}^3$  and  $40 \pm 3$ , respectively. Dicumyl peroxide (DCP; purity = 98%, MP =  $80 \text{ }^\circ\text{C}$ , Sigma-Aldrich Chemical Company, USA) was used as the curing agent.  $\text{TiO}_2$ ,  $\text{BaCO}_3$ ,  $\text{CaCO}_3$ ,  $\text{MgO}$ ,  $\text{SrCl}_2 \cdot 6\text{H}_2\text{O}$ , and  $\text{ZnO}$  were procured from Merck, India, whereas  $\text{La}_2\text{O}_3$  was procured from Alfa Aesar.

**2.2. Preparation of  $\text{La}_2\text{Ba}_2\text{XZn}_2\text{Ti}_3\text{O}_{14}$  ( $X = \text{Mg/Ca/Sr}$ ) Nanoparticles.**  $\text{La}_2\text{Ba}_2\text{XZn}_2\text{Ti}_3\text{O}_{14}$  ( $X = \text{Mg/Ca/Sr}$ ) [LBT ( $X = \text{Mg/Ca/Sr}$ )] nanoparticles are prepared through a high-temperature solid-state reaction using stoichiometric amounts of  $\text{BaCO}_3$ ,  $\text{TiO}_2$ ,  $\text{CaCO}_3$ ,  $\text{MgO}$ ,  $\text{SrCl}_2 \cdot 6\text{H}_2\text{O}$ ,  $\text{ZnO}$ , and  $\text{La}_2\text{O}_3$ . These ingredients were dried at  $150 \text{ }^\circ\text{C}$  for 6 h to remove the adsorbed moisture, and these dried oxides/hydroxides were thoroughly mixed in an agate mortar and loaded in an alumina boat/crucible. The mixture was heat-treated in a muffle furnace at  $700 \text{ }^\circ\text{C}$  for 6 h and  $1000 \text{ }^\circ\text{C}$  for 6 h, followed by heating at  $1200 \text{ }^\circ\text{C}$  (twice) for 6 and 2 h, respectively, with three intermittent grindings. The powder obtained was grinded thoroughly using an agate mortar before further study.

**2.3. Preparation of PDMS– $\text{La}_2\text{Ba}_2\text{XZn}_2\text{Ti}_3\text{O}_{14}$  ( $X = \text{Mg/Ca/Sr}$ ) (PDMS–LBT) Nanocomposites.** PDMS–LBT ( $X = \text{Mg/Ca/Sr}$ ) nanocomposites are prepared through a room-temperature mixing process, where LBT ( $X = \text{Mg/Ca/Sr}$ ) nanoparticles and other ingredients are mixed with the PDMS matrix in an internal mixer with a shear rate of 45 rpm for a mixing time of 10 min. The LBT ( $X = \text{Mg/Ca/Sr}$ ) nanoparticles and cross-linking agents are mixed with the pure matrix PDMS as per the formulations given in Table 1. Finally, these compounds were passed through a two-roll mill to make them into a sheet form. Composite designation:

**Table 1. Formulations of PDMS– $\text{La}_2\text{Ba}_2\text{XZn}_2\text{Ti}_3\text{O}_{14}$  (PDMS–LBT) Nanocomposites<sup>a</sup>**

ingredients	composition parts by weight per hundred parts of polymer (php)				
	P <sub>100</sub> LBT <sub>0</sub>	P <sub>100</sub> LBT <sub>10</sub>	P <sub>100</sub> LBT <sub>30</sub>	P <sub>100</sub> LBT <sub>50</sub>	P <sub>100</sub> LBT <sub>70</sub>
PDMS	100	100	100	100	100
LBT	0	10	30	50	70
DCP	1.5	1.5	1.5	1.5	1.5

<sup>a</sup>10 php = 9.09 wt %, 30 php = 23.08 wt %, 50 php = 33.34 wt %, and 70 php = 41.18 wt %.

P<sub>100</sub>LBT<sub>10</sub>, where P = PDMS and LBT =  $\text{La}_2\text{Ba}_2\text{XZn}_2\text{Ti}_3\text{O}_{14}$  nanoparticles. The optimum cure times of different compounds were evaluated by a rubber process analyzer (RPA) operating at  $150 \text{ }^\circ\text{C}$ . The different test specimens from all the composites were prepared using a compression molding press at  $150 \text{ }^\circ\text{C}$  and cured up to an optimum curing time of 5 min.

## 3. RESULTS AND DISCUSSION

**3.1. Properties of  $\text{La}_2\text{Ba}_2\text{XZn}_2\text{Ti}_3\text{O}_{14}$  ( $X = \text{Mg/Ca/Sr}$ ) Nanoparticles.** **3.1.1. X-ray Diffraction Analysis.** The XRD patterns of three different types of LBT ( $X = \text{Mg}, \text{Ca}, \text{or Sr}$ ) nanoparticles are shown in Figure 1. The XRD pattern of LBT nanoparticles ( $X = \text{Ca}$ ) well matched with the reported literature, whereas the other two particles ( $X = \text{Mg/Sr}$ ) showed similar XRD patterns.<sup>37</sup> It is observed that in all cases impurity peaks are observed for LBT particles prepared at  $1000 \text{ }^\circ\text{C}$ . However, these impurity peaks are absent in the case of particles prepared at  $1200 \text{ }^\circ\text{C}$ . Therefore, it can be concluded that  $1200 \text{ }^\circ\text{C}$  is the appropriate/optimum temperature for the preparation of LBT ( $X = \text{Mg/Ca/Sr}$ ) nanoparticles.

**3.1.2. Dielectric Properties.** Semilog plots of  $\log f$  vs dielectric constant ( $\epsilon'$ ) and dielectric loss ( $\epsilon''$ ) against frequency are shown in Figure 2. The prepared LBT ( $X = \text{Mg/Ca/Sr}$ ) nanoparticles have a high dielectric constant (permittivity) with a relatively low dielectric loss.

There is also an increase in both dielectric constant and dielectric loss with the decrease in frequency. The high dielectric constant at the low-frequency region is due to the presence of space charges, which undergo orientation during polarization. The low dielectric loss of this material, especially at high frequency, makes it suitable for applications such as capacitors and other electronic devices. It is also observed that LBT nanoparticles with “Ca” has a high dielectric constant compared to the other two LBT nanoparticles with “Mg” and “Sr”.

Figure 3 shows the temperature-dependent dielectric behavior of LBT ( $X = \text{Mg/Ca/Sr}$ ) nanoparticles at 1 kHz. It is observed that the dielectric constant of LBT ( $X = \text{Mg/Ca/Sr}$ ) nanoparticles changed with the increase in temperature due to the phase transition. The three different nanoparticles/oxides behave in a different manner with the increase in temperature. There is a significant increase in the dielectric constant at  $\sim 105 \text{ }^\circ\text{C}$  for LBT nanoparticles ( $X = \text{Sr}$ ), which is the Curie temperature of this material. Similarly, the dielectric constant of LBT nanoparticles ( $X = \text{Ca}$ ) is more in the temperature range of  $80\text{--}100 \text{ }^\circ\text{C}$ , which we can consider as its Curie point. Finally, LBT nanoparticles ( $X = \text{Mg}$ ) show a decrease in dielectric constant with the increase in temperature up to  $120 \text{ }^\circ\text{C}$ , but beyond  $120 \text{ }^\circ\text{C}$ , the dielectric constant again increases with the increase in temperature. It is also observed from the trend of the curve (Figure 3) that LBT nanoparticles

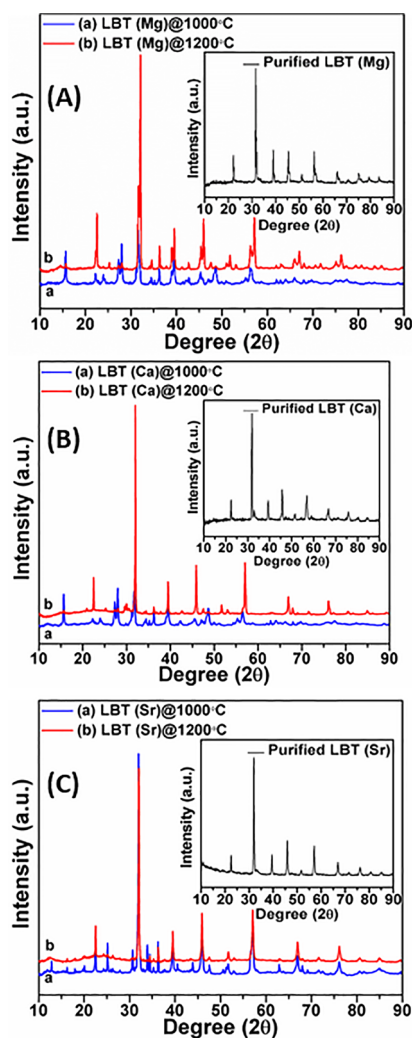


Figure 1. XRD patterns of (A–C)  $\text{La}_2\text{Ba}_2\text{XZn}_2\text{Ti}_3\text{O}_{14}$  ( $X = \text{Mg}/\text{Ca}/\text{Sr}$ ) nanoparticles.

( $X = \text{Mg}$ ) may have a high dielectric constant in the low-temperature range, so the Curie temperature of this material may be present at a low temperature. Due to the lack of measurement facility of the low-temperature dielectric study, the exact Curie temperature of LBT ( $X = \text{Mg}$ ) particles could not be determined in the present work and is for future research scope (low-temperature dielectric study of these oxide materials). The above types of oxide materials, especially LBT ( $X = \text{Sr}$ ) nanoparticles/oxides, can be used in dielectric/resistive switching devices.

**3.1.3. High-Resolution Transmission Electron Microscopy.** The shape and size of LBT ( $X = \text{Mg}/\text{Ca}/\text{Sr}$ ) nanoparticles can be seen from the HRTEM images in Figure 4. LBT ( $X = \text{Mg}/\text{Ca}$ ) nanoparticles are spherical in nature, where the size of particles is  $\sim 20$  nm, as clearly seen from the HRTEM images (Figure 4a,b). LBT ( $X = \text{Sr}$ ) nanoparticles are cubical in nature, where the size of particles is  $\geq 100$  nm (Figure 4c). These LBT ( $X = \text{Mg}/\text{Ca}/\text{Sr}$ ) nanoparticles are crystalline in nature, as is apparent from both the SAED (Figure 4d–f) and XRD (Figure 1A–C) patterns. From the SAED patterns, it is observed that LBT ( $X = \text{Mg}/\text{Ca}$ ) nanoparticles are crystalline (mixture of single- and polycrystalline) in nature, whereas LBT ( $X = \text{Sr}$ ) nanoparticles are single-crystalline in nature.

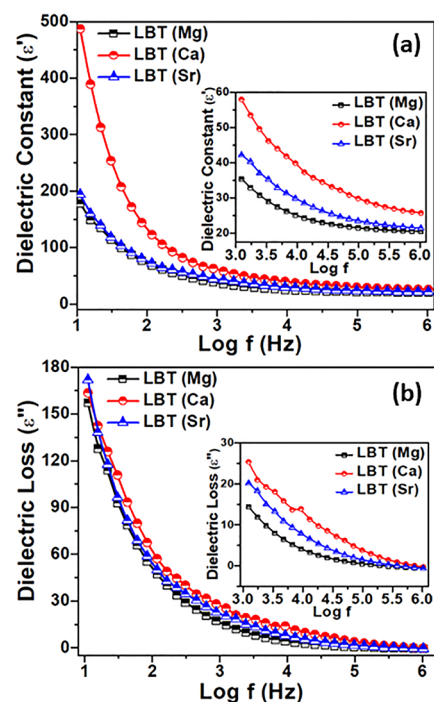


Figure 2. Variation of (a) dielectric constant and (b) dielectric loss against frequency for  $\text{La}_2\text{Ba}_2\text{XZn}_2\text{Ti}_3\text{O}_{14}$  ( $X = \text{Mg}/\text{Ca}/\text{Sr}$ ) nanoparticles.

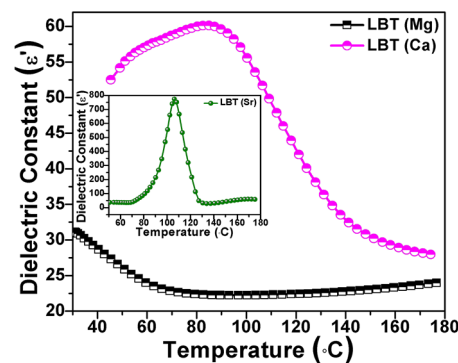
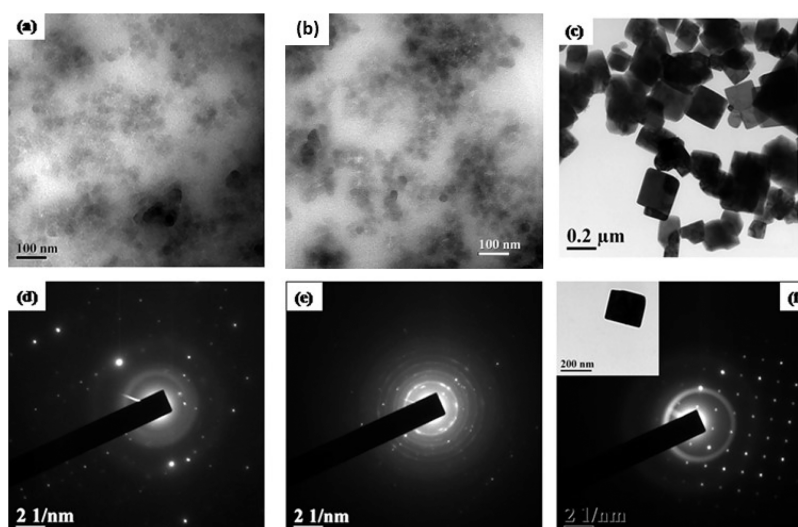


Figure 3. Variation of the dielectric constant with temperature at 1 kHz for  $\text{La}_2\text{Ba}_2\text{XZn}_2\text{Ti}_3\text{O}_{14}$  ( $X = \text{Mg}/\text{Ca}/\text{Sr}$ ) nanoparticles.

**3.1.4. Field Emission Scanning Electron Microscopy.** The presence of different elements (La, Ba, Mg, Ca, Sr, Zn, Ti, and O) in LBT ( $X = \text{Mg}/\text{Ca}/\text{Sr}$ ) nanoparticles is confirmed through FESEM-EDS analysis (Figure 5). The concentration of each element in LBT nanoparticles is also understood from the FESEM-EDS data given in Table 2.

**3.2. Properties of PDMS– $\text{La}_2\text{Ba}_2\text{XZn}_2\text{Ti}_3\text{O}_{14}$  ( $X = \text{Mg}/\text{Ca}/\text{Sr}$ ) Nanocomposites.**  
**3.2.1. Electrical Properties.** The DC resistivity of polymer composites depends on the resistivity of the matrix polymer as well as the particulate filler.<sup>39</sup> The DC resistivity of composites containing three types of filler particles [LBT ( $X = \text{Mg}/\text{Ca}/\text{Sr}$ )] is presented in Figure 6. There is a gradual decrease in DC resistivity with an increase in the filler concentration, as observed from the figure. The steady decrease in the volume resistivity with the increase in filler concentration is due to the low resistivity of the LBT nanoparticles, as compared with the matrix PDMS. Moreover, inorganic oxide particles usually contain some amount of moisture; as a result, with the increase in the filler



**Figure 4.** HRTEM images and SAED patterns of (a, d) LBT ( $X = \text{Mg}$ ), (b, e) LBT ( $X = \text{Ca}$ ), and (c, f) LBT ( $X = \text{Sr}$ ) nanoparticles.

**Table 2.** SEM-EDX Data for  $\text{La}_2\text{Ba}_2\text{XZn}_2\text{Ti}_3\text{O}_{14}$  ( $X = \text{Mg}/\text{Ca}/\text{Sr}$ ) Nanoparticles

$\text{La}_2\text{Ba}_2\text{CaZn}_2\text{Ti}_3\text{O}_{14}$			$\text{La}_2\text{Ba}_2\text{MgZn}_2\text{Ti}_3\text{O}_{14}$			$\text{La}_2\text{Ba}_2\text{SrZn}_2\text{Ti}_3\text{O}_{14}$		
element	weight %	atomic %	element	weight %	atomic %	element	weight %	atomic %
O	30.56	70.47	O	38.54	77.63	O	31.45	73.89
Ca	2.75	2.54	Mg	3.18	4.22	Sr	2.64	2.47
Ti	14.36	11.06	Ti	8.36	5.62	Ti	7.84	10.57
Zn	6.65	3.75	Zn	3.60	1.77	Zn	5.39	3.28
Ba	18.40	4.94	Ba	6.29	1.48	Ba	20.37	3.63
La	27.28	7.24	La	40.03	9.29	La	32.31	6.16
total	100.00		total	100.00		total	100.00	

concentration, the DC resistivity of the composites is decreased. The presence of moisture on these filler surfaces helps in the ionization of ionic species in the composite system, which decreases the electrical resistivity of composites. It is also observed from the figure that composites with LBT ( $X = \text{Ca}$ ) particles have low resistivity than the composites prepared from the other two fillers (LBT ( $X = \text{Mg}/\text{Sr}$ )).

The variation of dielectric constant against frequency for both pure PDMS and PDMS–LBT ( $X = \text{Mg}/\text{Ca}/\text{Sr}$ ) nanocomposites with two concentrations (9.09 and 41.18 wt %) has been presented in Figure 7. There is an increase in the dielectric constant with the decrease in frequency for composites containing three types of fillers. The high dielectric constant at the low-frequency region is due to the interfacial and dipolar polarization. The change in dielectric constant is also composition-dependent over the entire frequency range. As discussed above, LBT ( $X = \text{Ca}$ ) nanoparticles have the highest dielectric constant value, whereas LBT ( $X = \text{Mg}$ ) nanoparticles have the lowest value. We also have observed a similar trend in the case of composites prepared from these fillers. In the case of composites at a concentration (say 41.18 wt %) of the filler, the composite with LBT ( $X = \text{Ca}$ ) nanoparticles has the highest dielectric constant and the composite with LBT ( $X = \text{Mg}$ ) nanoparticles has the lowest value.

The effect of temperature on the frequency (1 kHz)-dependent AC conductivity and dielectric constant of composites (41.18 wt %) is shown in Figure 8. There is an increase in dielectric constant and conductivity with the increase in temperature, as observed from Figure 8. The

increase in conductivity and dielectric constant of the composites with the increase in temperature is due to the increase in the net polarization. There is a change in trend in the case of composites prepared from LBT ( $X = \text{Sr}$ ) nanoparticles and a sudden increase in dielectric constant/conductivity above 100 °C. This is due to the Curie temperature ( $\sim 105$  °C) of LBT ( $X = \text{Sr}$ ) nanoparticles, as observed in Figure 3.

**3.2.2. Mechanical Properties.** The variation of percent elongation at break (% EB) and tensile strength (TS) for different PDMS–LBT ( $X = \text{Mg}/\text{Ca}/\text{Sr}$ ) nanocomposites against the filler concentration is presented in Figure 9a,b. The continuous decrease in both % EB and TS with the increase in LBT ( $X = \text{Mg}/\text{Ca}/\text{Sr}$ ) nanoparticle concentration in the matrix PDMS indicates that these three types of filler particles are nonreinforcing in nature for the matrix PDMS.

It is also observed that composites filled with LBT ( $X = \text{Sr}$ ) particles have more TS and % EB as compared to the composites prepared from the other two filler particles (LBT ( $X = \text{Mg}/\text{Ca}$ )). The higher tensile strength and % EB in the case of composites filled with LBT ( $X = \text{Sr}$ ) particles may be due to better polymer–filler interaction as compared to other composites. There is a continuous increase in hardness (Figure 9c) with the increase in the concentration of LBT ( $X = \text{Mg}/\text{Ca}/\text{Sr}$ ) nanoparticles, which is due to the restricted movement of polymer chains. The decrease in tear strength with the increase in filler concentration is due to the increase in the number of particle clusters in the matrix polymer which generates a path for crack propagation (Figure 9d).

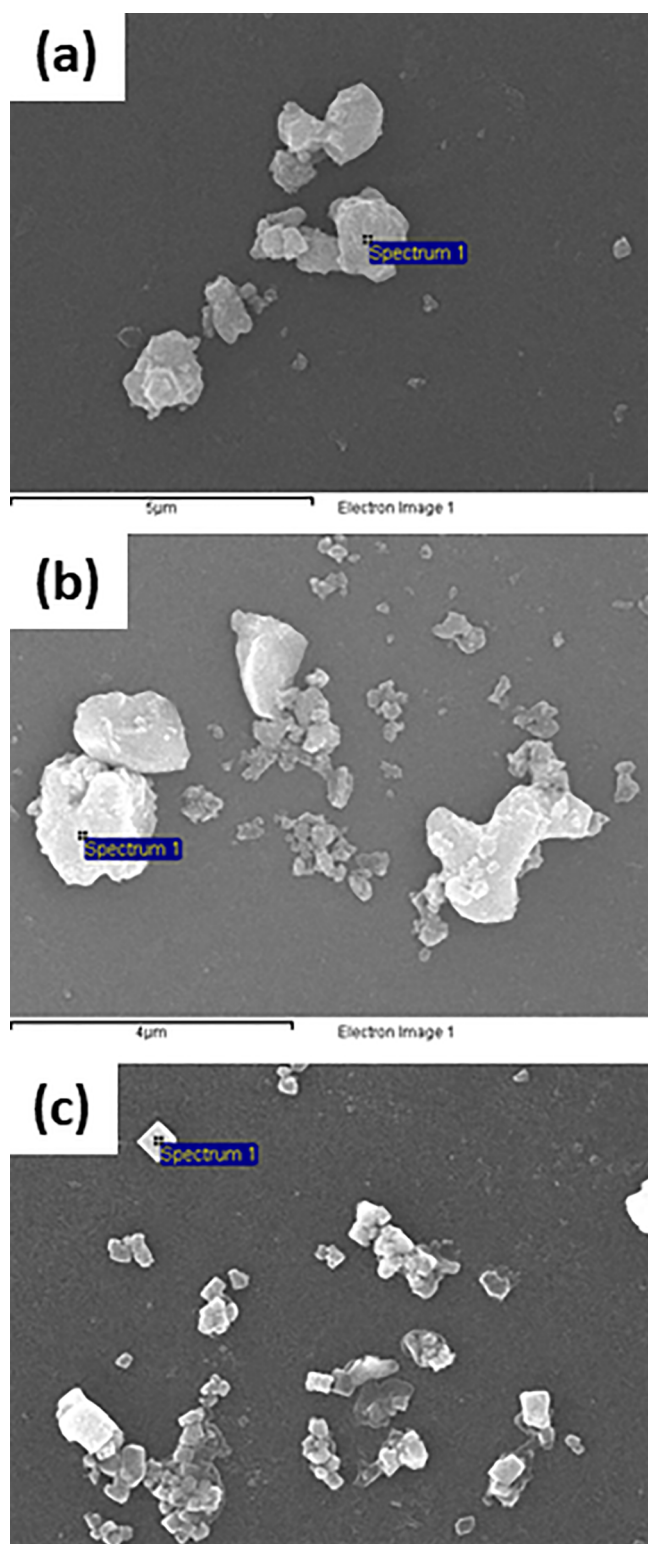


**Figure 5.** FESEM-EDS images of (a) LBT ( $X = \text{Ca}$ ), (b) LBT ( $X = \text{Mg}$ ), and (c) LBT ( $X = \text{Sr}$ ) nanoparticles.

**3.2.3. Morphological Analysis via HRTEM and AFM.** The HRTEM images of nanocomposites containing 23.08 wt % of three different types of LBT ( $X = \text{Mg}/\text{Ca}/\text{Sr}$ ) nanoparticles are presented in Figure 10a–c. The distribution of LBT nanoparticles is good in all the cases, whereas particle dispersion is better in the case of the composite containing LBT ( $X = \text{Mg}$ ) nanoparticles than the composites containing

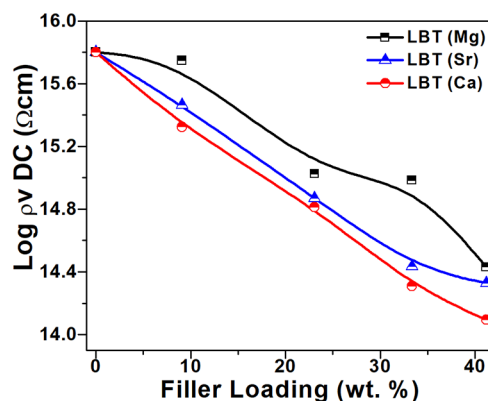


**Figure 6.** Effect of the LBT ( $X = \text{Mg}/\text{Ca}/\text{Sr}$ ) filler concentration on DC volume resistivity.

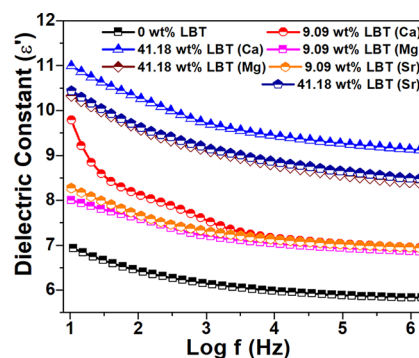


**Figure 7.** Semilog plot of dielectric constant ( $\epsilon'$ ) against frequency for different composites.

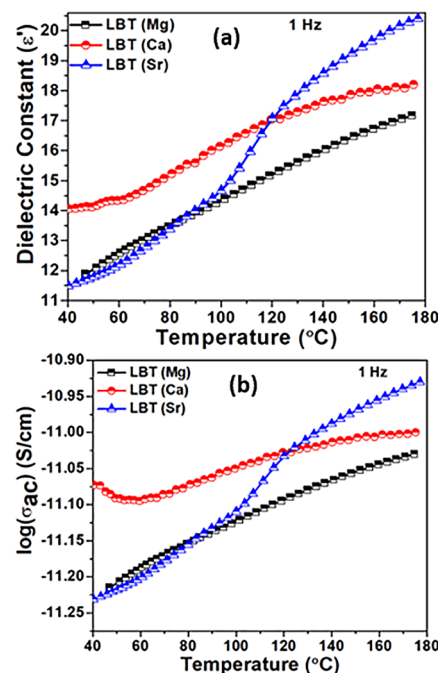


**Figure 8.** Effect of temperature on (a) dielectric constant and (b) AC conductivity of composites at a frequency of 1 Hz.

LBT ( $X = \text{Ca}/\text{Sr}$ ) nanoparticles. It is apparent from these figures that the shape of nanoparticles is spherical in nature, and the particle size is  $\sim 20$  nm.

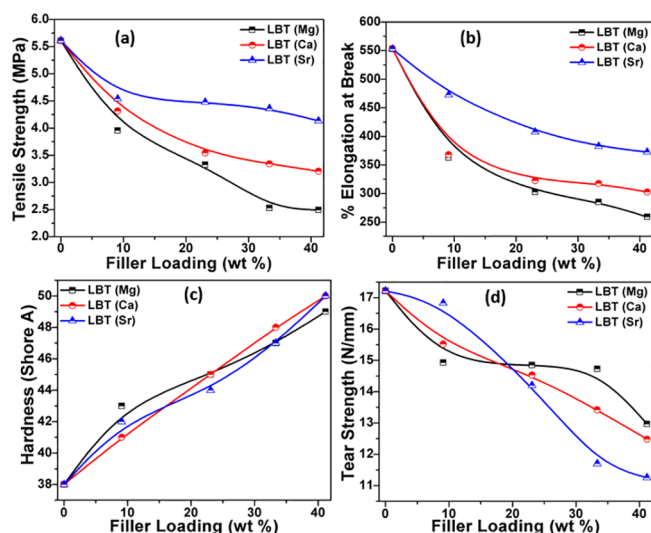


**Figure 9.** Variation of (a) tensile strength, (b) % elongation at break, (c) hardness, and (d) tear strength against the filler concentration of different PDMS– $\text{La}_2\text{Ba}_2\text{XZn}_2\text{Ti}_3\text{O}_{14}$  ( $\text{X} = \text{Mg}/\text{Ca}/\text{Sr}$ ) composites.

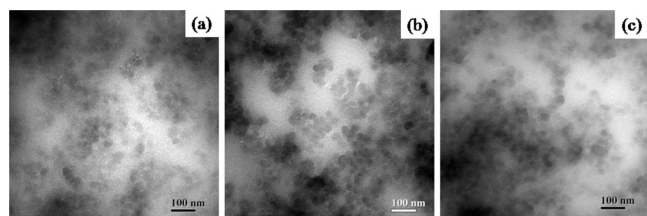


**Figure 10.** HRTEM images of (a) PDMS + 23.08 wt % LBT ( $\text{X} = \text{Mg}$ ), (b) PDMS + 23.08 wt % LBT ( $\text{X} = \text{Ca}$ ), and (c) PDMS + 23.08 wt % LBT ( $\text{X} = \text{Sr}$ ) composites.

The particle distribution and dispersion can be understood from the AFM images. Figure 11a,b represents the tapping mode 2D and 3D images of PDMS–LBT ( $\text{X} = \text{Sr}$ ) nanocomposites containing 23.08 wt % of LBT ( $\text{X} = \text{Sr}$ ) nanoparticles, and their corresponding height profiles are shown in Figure 11c,d. The height profile of the PDMS–LBT ( $\text{X} = \text{Sr}$ ) nanocomposite confirms the thorough distribution of LBT ( $\text{X} = \text{Sr}$ ) particles (positions 1, 2, and 3) in the matrix PDMS. The height profile of the nanocomposite along the line drawn on the picture is shown in Figure 11c. The presence of LBT ( $\text{X} = \text{Sr}$ ) particles in different locations can be detected, e.g., particles with height  $\sim 62$  nm (position 1), particles with height  $\sim 66$  nm (position 2), and particles with height  $\sim 53$  nm (position 3).

#### 4. SUMMARY AND CONCLUSIONS

The formation of  $\text{La}_2\text{Ba}_2\text{XZn}_2\text{Ti}_3\text{O}_{14}$  ( $\text{X} = \text{Mg}/\text{Ca}/\text{Sr}$ ) nanoparticles is confirmed through X-ray diffraction and SEM-EDS analysis. The shape of LBT ( $\text{X} = \text{Sr}$ ) nanoparticles is cubical in shape, with size  $\geq 100$  nm, whereas the other two particles (LBT ( $\text{X} = \text{Mg}/\text{Ca}$ )) are spherical in shape with size  $\sim 20$  nm, as clearly seen from the HRTEM images. These nanoparticles are crystalline in nature, as confirmed through SAED analysis and X-ray diffraction. The dielectric constant of LBT ( $\text{X} = \text{Ca}$ ) particles and composites containing LBT ( $\text{X} = \text{Ca}$ ) particles are more than that of the other two particles (LBT ( $\text{X} = \text{Mg}/\text{Sr}$ )). The dielectric measurement reveals that the dielectric loss of these particles is less than the dielectric constant, especially at high-frequency regions. Different particles behave differently with the increase in temperature, and they have different Curie temperatures. These kinds of oxide materials, especially LBT ( $\text{X} = \text{Sr}$ ) nanoparticles/oxides, can be used in dielectric/resistive switching devices. PDMS–LBT ( $\text{X} = \text{Mg}/\text{Ca}/\text{Sr}$ ) nanocomposites show both composition- and frequency-dependent dielectric properties. The LBT

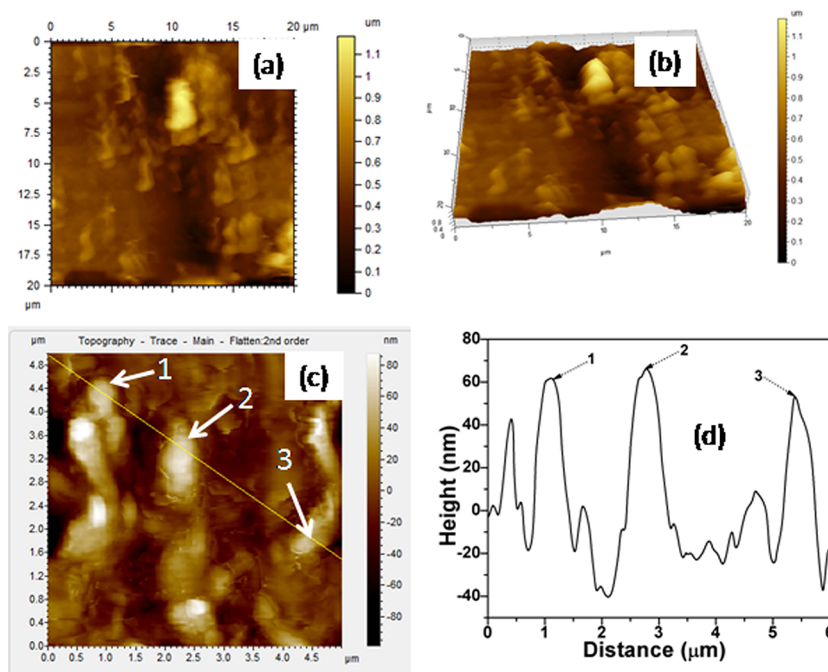


**Figure 11.** AFM/SPM (a, c) 2D and (b) 3D images and (d) height profiling of PDMS– $\text{La}_2\text{Ba}_2\text{XZn}_2\text{Ti}_3\text{O}_{14}$  ( $\text{X} = \text{Sr}$ ) composites containing 23.08 wt % LBT ( $\text{X} = \text{Sr}$ ) nanoparticles.

(X = Mg/Ca/Sr) nanoparticles are nonreinforcing fillers for the matrix PDMS. The nanocomposites with LBT (X = Ca) nanoparticles have low resistivity (high conductivity) than the composites prepared from the other two fillers (LBT (X = Mg/Sr)).

## AUTHOR INFORMATION

### Corresponding Author

**Suryakanta Nayak** – Rubber Technology Centre, Indian Institute of Technology, Kharagpur, West Bengal 721302, India; Department of Mechanical Engineering, National University of Singapore, Singapore 117575, Singapore; Department of Electrical and Computer Engineering, National University of Singapore, Singapore 117583, Singapore; R&D, Surface Engineering Research Group, Tata Steel Limited, Jamshedpur 831001, India; [orcid.org/0000-0001-5189-5519](https://orcid.org/0000-0001-5189-5519); Phone: +91 86586 26626; Email: [suryakanta.nayak@tatasteel.com](mailto:suryakanta.nayak@tatasteel.com), [suryakanta.nus@gmail.com](mailto:suryakanta.nus@gmail.com)

### Authors

**Banalata Sahoo** – Department of Chemistry, Indian Institute of Technology, Kharagpur, West Bengal 721302, India; Department of Chemistry, Regional Institute of Education, Bhubaneswar, Odisha 751022, India; Present Address: Department of Chemistry, Binayak Acharya Degree College, Berhampur, Odisha 760006, India  
**Tapan Kumar Rout** – R&D, Surface Engineering Research Group, Tata Steel Limited, Jamshedpur 831001, India  
**Amar Nath Bhagat** – R&D, Surface Engineering Research Group, Tata Steel Limited, Jamshedpur 831001, India

Complete contact information is available at:

<https://pubs.acs.org/10.1021/acsomega.3c04538>

### Author Contributions

<sup>‡</sup>S.N. and B.S. contributed equally.

### Notes

The authors declare no competing financial interest.

## ACKNOWLEDGMENTS

The authors would like to thank Indian Institute of Technology Kharagpur, India, for providing research facility. The authors are also thankful to Prof. Panchanan Pramanik (Retd. from Department of Chemistry, IIT Kharagpur, India) for providing his high-temperature furnace facility.

## REFERENCES

- (1) Nayak, S.; Kumar Chaki, T.; Khashtgir, D. In Development of poly (dimethylsiloxane)/BaTiO<sub>3</sub> nanocomposites as dielectric material. *Adv. Mater. Res.* **2012**, *622-623*, 897–900.
- (2) Ramajo, L.; Castro, M. S.; Reboredo, M. M. Dielectric response of Ag/BaTiO<sub>3</sub>/epoxy nanocomposites. *J. Mater. Sci.* **2010**, *45* (1), 106–111.
- (3) Nayak, S.; Chaki, T. K.; Khashtgir, D. Development of flexible piezoelectric poly (dimethylsiloxane)–BaTiO<sub>3</sub> nanocomposites for electrical energy harvesting. *Ind. Eng. Chem. Res.* **2014**, *53* (39), 14982–14992.
- (4) Bandyopadhyay, S.; Al-Juhani, A.; Girei, S. A.; Thomas, S. P.; Atieh, M. A.; Mezghani, K.; De, S. *Journal of Thermoplastic.*
- (5) Gunes, I. S.; Cao, F.; Jana, S. C. Evaluation of nanoparticulate fillers for development of shape memory polyurethane nanocomposites. *Polymer* **2008**, *49* (9), 2223–2234.
- (6) Liang, G.; Tjong, S. Electrical properties of low-density polyethylene/multiwalled carbon nanotube nanocomposites. *Mater. Chem. Phys.* **2006**, *100* (1), 132–137.
- (7) Patel, H. A.; Somani, R. S.; Bajaj, H. C.; Jasra, R. V. Nanoclays for polymer nanocomposites, paints, inks, greases and cosmetics formulations, drug delivery vehicle and waste water treatment. *Bull. Mater. Sci.* **2006**, *29* (2), 133–145.
- (8) Nayak, S.; Rahaman, M.; Pandey, A.; Setua, D. K.; Chaki, T. K.; Khashtgir, D. Development of poly (dimethylsiloxane)–titania nanocomposites with controlled dielectric properties: effect of heat treatment of titania on electrical properties. *J. Appl. Polym. Sci.* **2013**, *127* (1), 784–796.
- (9) Nayak, S.; Sahoo, B.; Chaki, T. K.; Khashtgir, D. Development of polyurethane–titania nanocomposites as dielectric and piezoelectric material. *RSC Adv.* **2013**, *3* (8), 2620–2631.
- (10) Lamorinière, S.; Jones, M. P.; Ho, K.; Kalinka, G.; Shaffer, M. S.; Bismarck, A. Carbon nanotube enhanced carbon Fibre-Poly (ether ether ketone) interfaces in model hierarchical composites. *Compos. Sci. Technol.* **2022**, *221*, No. 109327.
- (11) Cai, J. H.; Huang, M. L.; Chen, X. D.; Wang, M. Controllable construction of cross-linking network for regulating on the mechanical properties of polydimethylsiloxane and polydimethylsiloxane/carbon nanotubes composites. *J. Appl. Polym. Sci.* **2022**, *139* (19), 52113.
- (12) Ketikis, P.; Damopoulos, E.; Pilatos, G.; Klonos, P.; Kyritsis, A.; Tarantili, P. A. Preparation by solution mixing and characterization of condensation type poly (dimethyl siloxane)/graphene nanoplatelets composites. *J. Compos. Mater.* **2022**, *56* (2), 251–266.
- (13) Nayak, S.; Chaki, T. K.; Khashtgir, D. Spherical ferroelectric PbZr<sub>0.52</sub>Ti<sub>0.48</sub>O<sub>3</sub> nanoparticles with high permittivity: Switchable dielectric phase transition with temperature. *Ceram. Int.* **2016**, *42* (13), 14490–14498.
- (14) Nayak, S.; Sahoo, B.; Chaki, T. K.; Khashtgir, D. Facile preparation of uniform barium titanate (BaTiO<sub>3</sub>) multipods with high permittivity: impedance and temperature dependent dielectric behavior. *RSC Adv.* **2014**, *4* (3), 1212–1224.
- (15) Nayak, S. Dielectric properties of polymer–carbon composites. *Carbon-Containing Polym. Compos.* **2019**, 211–234.
- (16) Bhandari, S.; Nayak, S.; Artiaga, R.; Guchhait, P. K. Time derivative of DSC and dielectric analysis of elastomeric poly (thiourethane–urethane)/Cloisite 30B clay nanocomposites. *Iran. Polym. J.* **2023**, *32* (2), 151–163.
- (17) Nayak, S.; Khashtgir, D. Polydimethylsiloxane–PbZr<sub>0.52</sub>Ti<sub>0.48</sub>O<sub>3</sub> nanocomposites with high permittivity: Effect of poling and temperature on dielectric properties. *J. Appl. Polym. Sci.* **2019**, *136* (14), 47307.
- (18) Nayak, S.; Chaki, T. K.; Khashtgir, D. Dielectric relaxation and viscoelastic behavior of polyurethane–titania composites: dielectric mixing models to explain experimental results. *Polym. Bull.* **2017**, *74*, 369–392.
- (19) Manna, R.; Nayak, S.; Rahaman, M.; Khashtgir, D. Effect of annealed titania on dielectric and mechanical properties of ethylene propylene diene monomer-titania nanocomposites. *e-Polymers* **2014**, *14* (4), 267–275.
- (20) Adireddy, S.; Puli, V. S.; Lou, T. J.; Elupula, R.; Sklare, S.; Riggs, B. C.; Chrisey, D. B. Polymer-ceramic nanocomposites for high energy density applications. *J. Sol-Gel Sci. Technol.* **2015**, *73* (3), 641–646.
- (21) Zheng, J.; Hu, Y.-Y. New insights into the compositional dependence of Li-ion transport in polymer–ceramic composite electrolytes. *ACS Appl. Mater. Interfaces* **2018**, *10* (4), 4113–4120.
- (22) Palmer, M. J.; Kalnaus, S.; Dixit, M. B.; Westover, A. S.; Hatzell, K. B.; Dudney, N. J.; Chen, X. C. A three-dimensional interconnected polymer/ceramic composite as a thin film solid electrolyte. *Energy Storage Mater.* **2020**, *26*, 242–249.
- (23) Huang, B.; Caetano, G.; Vyas, C.; Blaker, J. J.; Diver, C.; Bártolo, P. Polymer-ceramic composite scaffolds: The effect of hydroxyapatite and β-tri-calcium phosphate. *Materials* **2018**, *11* (1), 129.

- (24) Huang, Y.; Wan, C. Controllable fabrication and multifunctional applications of graphene/ceramic composites. *J. Adv. Ceram.* **2020**, *9* (3), 271–291.
- (25) Zhu, H.; Liu, G.; Yuan, J.; Chen, T.; Xin, F.; Jiang, M.; Fan, Y.; Jin, W. In-situ recovery of bio-butanol from glycerol fermentation using PDMS/ceramic composite membrane. *Sep. Purif. Technol.* **2019**, *229*, No. 115811.
- (26) Mukherjee, D.; Banerjee, S.; Ghosh, S.; Majumdar, S. PDMS/ceramic composite membrane synthesis and evaluation of ciprofloxacin removal efficiency. *Korean J. Chem. Eng.* **2020**, *37* (11), 1985–1998.
- (27) Mathews, J. M.; Ananthakumar, S. Investigations on the Evolution of Zn Dust into ZnO Nanostructures. In *Electroceramics and Polymer Matrix Composite Dielectrics*; Cochin University of Science and Technology, 2019.
- (28) Geyer, R. G.; Asadi-Zeydabadi, M. Tailored dielectric and magnetic properties of composite electroceramics with ferroelectric and ferrimagnetic components. *J. Appl. Phys.* **2018**, *124* (16), 164104.
- (29) Kamble, R. B. *Tuning of electrical and magnetic properties in nanocomposites of conductive LaNiO<sub>3</sub> and transition metal oxides*, 2021.
- (30) Hwangbo, S.; No, H.-G.; Son, B.-R.; Hwang, K.-S. Structural and Electrical Properties of Solution Casted-BaTiO<sub>3</sub>-Polyvinylidene Composite Layers. *J. Nanosci. Nanotechnol.* **2020**, *20* (1), 568–572.
- (31) Stuber, V. L.; Mahon, T. R.; Van der Zwaag, S.; Groen, P. The effect of the intrinsic electrical matrix conductivity on the piezoelectric charge constant of piezoelectric composites. *Mater. Res. Express* **2020**, *7* (1), No. 015703.
- (32) Hashim, A.; Hadi, Q. Structural, electrical and optical properties of (biopolymer blend/titanium carbide) nanocomposites for low cost humidity sensors. *J. Mater. Sci.: Mater. Electron.* **2018**, *29* (13), 11598–11604.
- (33) Salame, P. H.; Kolte, J. T. Role of lanthanide substitution on suitable sites in enhancing the properties of various electroceramics. In *Spectroscopy of Lanthanide Doped Oxide Materials*; Elsevier, 2020; pp 365–392.
- (34) Moulson, A. J.; Herbert, J. M. *Electroceramics: materials, properties, applications*; John Wiley & Sons, 2003.
- (35) Nayak, S.; Li, Y.; Tay, W.; Zamburg, E.; Singh, D.; Lee, C.; Koh, S. J. A.; Chia, P.; Thean, A. V.-Y. Liquid-metal-elastomer foam for moldable multi-functional triboelectric energy harvesting and force sensing. *Nano Energy* **2019**, *64*, No. 103912.
- (36) Nayak, S.; Sahoo, B.; Khastgir, D. Flexible Nanocomposites Comprised of Poly(dimethylsiloxane) and High-Permittivity TiO<sub>2</sub> Nanoparticles Doped with La<sup>3+</sup>/Cu<sup>+</sup> for Dielectric Applications. *ACS Appl. Nano Mater.* **2019**, *2* (7), 4211–4221.
- (37) Jha, P.; Ganguli, A. K. New perovskite-related oxides having high dielectric constant: Ln<sub>2</sub>Ba<sub>2</sub>CaZn<sub>2</sub>Ti<sub>3</sub>O<sub>14</sub> (Ln = La and Pr). *J. Chem. Sci.* **2003**, *115* (5), 431–438.
- (38) Jha, P.; Bobev, S.; Subbanna, G. N.; Ganguli, A. K. Nd<sub>2</sub>Ba<sub>2</sub>CaZn<sub>2</sub>Ti<sub>3</sub>O<sub>14.4</sub>: A New High Dielectric Constant Oxide Having a Disordered (Cubic) Perovskite Structure. *Chem. Mater.* **2003**, *15* (11), 2229–2233.
- (39) Rahaman, M.; Chaki, T. K.; Khastgir, D. Development of high performance EMI shielding material from EVA, NBR, and their blends: effect of carbon black structure. *J. Mater. Sci.* **2011**, *46* (11), 3989–3999.